# Status and Perspectives of High Field Magnets for Particle Accelerators

Ezio Todesco

***Abstract*—Superconducting magnets have been an enabling technology for particle accelerators for more than 40 years. An introduction on the specific challenges of high field accelerator dipoles with respect to other devices, such as solenoids or detector magnets, will be provided followed by a brief historical overview of the development of Nb-Ti magnets for particle colliders, up to the 8 T dipole fields achieved in the LHC at 1.9 K. $Nb_3Sn$ was considered as an option for LHC; we will recall the development of $Nb_3Sn$ dipole short models in the 10–14 T range in the past 35 years. The focus will then shift to the present status of $Nb_3Sn$ technology used in the quadrupoles to be installed at CERN in the High Luminosity LHC at the end of this decade, with 11.5 T operational peak field and lengths up to 7.5 m. To continue, the developments of $Nb_3Sn$ dipoles for future colliders aiming at an operational field of the order of 14 T will be discussed. High Temperature Superconductors are used as current leads in the LHC and are planned for the HL-LHC: we will give an outlook on the opportunities and challenges of making dipole magnets using HTS, to achieve fields of the order of 20 T.**

***Index Terms*—Superconducting magnets, dipole magnets, particle accelerators, high-energy colliders.**

## I. Introduction

SUPERCONDUCTIVITY and its applications are an interesting paradigm in the history of physics and technology. The discovery of 1911 was made possible thanks to the achievement of a major technological challenge: the liquefaction of helium. It is worth noting that the motivation of the Nobel prize, awarded to K. Onnes only two years later, quotes helium liquefaction, but does not explicitly mention superconductivity, thus giving the leading role to a technological achievement rather than to the discovery itself. The second remarkable aspect is that the development of theories for superconductivity lagged behind experimental results, sometimes by several decades. Thirdly, applications to build superconducting magnets of the order of 1 tesla arrived only 50 years after the Onnes Nobel prize [1]: this shows that sometimes one has to be extremely patient and very determined to get technological applications from basic science discoveries.

Superconducting magnets giving more than 1 Tesla were finally built in the 60's: 4 T were achieved in 1961 [2] and 10 T in 1964 [3] (see [1] for an historical overview). What has been blocking for five decades is that type-I superconductors cannot withstand magnetic fields above a few mT, and that for type-II superconductors, discovered in 1935 and allowing magnetic flux penetration, a bulk wire cannot withstand large magnetic fields (by large we mean order of 1 T). Type-II superconductors have to be mixed with a good conductor to reduce the minimum quench energy, and have to be drawn to fine filaments to avoid instabilities caused by the magnetization induced by screening currents. This second aspect requires a very complex architecture for superconducting wires. The equation giving an estimate of the maximum dimension $d$ of a stable superconducting filament is

$$d < \frac{2}{j_c}\sqrt{\frac{3\gamma C_p(T_{cs}-T)}{\mu_0}}; \tag{1}$$

replacing the typical values for a low temperature superconductor, i.e., a volumetric specific heat $\gamma C_p$ of 2000 J/K/m$^3$ at a temperature of few kelvins, a critical current density $j_c$ at low field of $10^4$ A/mm$^2$, and a temperature margin ($T_{cs}$-$T$) of 10 K, one gets $d$<0.03 mm. We will come back to this equation in the last section of this paper, devoted to the perspectives for High Temperature Superconductors (HTS) for applications to accelerator magnets.

The technological achievements of the 60's rapidly entered the collective imagination: in 1974, ten years after the construction of the first superconducting magnets giving 10 T, in the ninth 007 movie [4], James Bond discusses with Mr. Scaramanga about "superconductive coils cooled in liquid helium used to store energy" (to power a very destructive laser). Mr. Scaramanga gets killed in a beautiful psychedelic scene during a duel with James Bond, but his bodyguard obviously fell in an open-air pool of liquid helium. Liquid nitrogen would have been more correct from a cryogenic point of view, but HTS would be discovered only ten years later.

In the same years of the Hollywood blockbuster, the first superconducting magnets to be installed in an accelerator were developed at CERN: eight large aperture quadrupoles based on Nb-Ti conductor, giving 43 T/m in a 173 mm diameter bore, with a peak field of 5.8 T, and 1-m-magnetic length [5]. These magnets were needed to allow smaller beam size in the Interaction Region (IR), thus increasing the number of collisions.

The IR quadrupoles of ISR operated for a decade, and were followed by the construction and installation of magnets based on a similar design in LEP-I and LEP-II [6], [7]. IR quadrupoles optical function becomes significant only at top energy, thus imposing less stringent requirements on magnet reproducibility and field quality with respect to a bending dipole: for this reason,

Received 1 December 2024; revised 2 February 2025; accepted 20 February 2025. Date of publication 4 April 2025; date of current version 5 May 2025.

The author is with TE Department, CERN, 1211 Geneva, Switzerland (e-mail: ezio.todesco@cern.ch).

Color versions of one or more figures in this article are available at https://doi.org/10.1109/TASC.2025.3558196.

Digital Object Identifier 10.1109/TASC.2025.3558196

these magnets featured a coil design based on a rectangular wire stacked in rectangular blocks. This path has been abandoned for the magnets of the following accelerators, based on Rutherford cable, but has been used in correctors for the LHC [8].

This paper gives an overview of superconducting magnets for particle accelerators, with a special focus on the design and tests. It will follow the *fil rouge* of the overall current density (aka the current density over the insulated coil), that is one of the most significant magnet design parameters, both from a purely electromagnetic and from a superconducting point of view. Advances in superconductors properties, manufacturing techniques, and other aspects are not discussed here for the sake of brevity.

The paper is structured as follows: after recalling the specificity of main superconducting magnets for accelerators, we briefly outline in Section III the development of Nb-Ti technology in colliders from the Tevatron to the LHC. In Section IV we discuss the progress in short model dipoles based on $Nb_3Sn$ technology from the 90's to the 10's, approaching 15 T. Section V is devoted to the scaling of the $Nb_3Sn$ technology from 1.5 m to 7 m carried out in the framework of the HL-LHC project, the first one aiming to install this technology in an accelerator. In Section VI we outline the requirements for future colliders giving 100 TeV center of mass energies, such as FCC-hh and SppC, and the development lines that are being followed in the US, in Europe and in China. Finally, Section VII is devoted to an outlook of the possible use of HTS for accelerator magnets.

## II. Features of Superconducting Magnets for Hadron Accelerators

### A. High Field Dipoles for High Energy Hadron Accelerators

The energy that can be achieved in a synchrotron accelerator of curvature radius $\rho$ and magnetic field $B$ for a particle with the charge of a proton is given by

$$E\,[GeV] = 0.3 \times B\,[\mathrm{T}]\,\rho\,[\mathrm{m}]\,. \tag{2}$$

A synchrotron has two paradoxes: even though the magnetic field plays no role in the acceleration, for a given diameter the limit to the energy is given by $B$. In fact, one can go through the accelerating sector as long as the field increase is synchronized with the energy increase to stay on the orbit of curvature radius $\rho$: the maximum energy is therefore given by the maximum field in the dipoles. Moreover, the accelerating section is very small (order of meters) with respect to the size of the machine (order of km), and therefore it is a second-order component of the cost, which is dominated by the magnets.

Applying (2) to the LHC case, one has 8.3 T field and 2.8 km curvature radius, thus giving 7.0 TeV energy per beam. The circumference relative to the 2.8 km curvature radius is 17.6 km. Note that the total circumference of the LHC tunnel is much longer (26.7 km): it is made of 22.0 km of arcs (curved sections) and 4.7 km of straight sections, where the four experiments are located. The ratio 17.6/22.0 = 0.80 is the filling factor of the arcs, i.e., 80% of the arcs covered by a dipolar field. The remaining 20% gives space to quadrupoles (7%), correctors, and interconnections. Two main paths are given to increase the particle energy in a synchrotron: longer accelerators and/or higher fields. However, increasing the filling factor gives a second order contribution (order of 10%) to the global optimization of the system [9]; this can become significant when the dipole field is pushed at the limits of the associated superconducting technology.

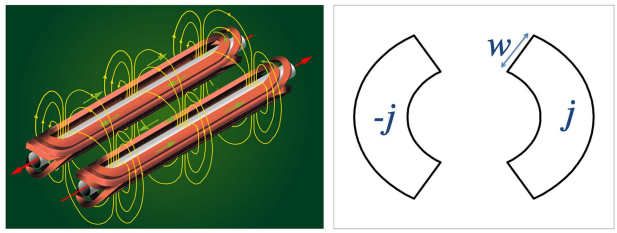


Fig. 1. Schematic view of a dipole magnet based on cos$\theta$ geometry: 3D view (left) and cross-section (right).

### B. Field Versus Current Density and Coil Width

A dipolar field can be generated in a aperture with the sector coil configuration as shown in Fig. 1; the field is approximately given by the product of the overall current density (aka current over the insulated winding, see also the appendix for definitions) times the width of the coil, weighted by half of the vacuum magnetic permeability:

$$B\,[\mathrm{T}] \approx \frac{1}{2}\mu_0 jw = 0.00063j\,\left[\mathrm{A/mm^2}\right] w\,[\mathrm{mm}]\,. \tag{3}$$

For a 60° sector coil as shown in Fig. 1, the ratio between field and $jw$ is 10% larger, i.e., ~0.00070 T mm/A. Note that the field is independent of the aperture. In solenoids, one has 50% more conductor (thus covering the whole bore tube with the winding, that is perpendicular to the beam axis) and twice the field (i.e., the weight factor is $\mu_0$ and not $\mu_0/2$). Therefore, a solenoid has a 33% larger efficiency w.r.t. a dipole in producing field for a given quantity of conductor.

### C. The Superconducting Leap

Electromagnets based on copper or aluminum are limited to 1–5 A/mm$^2$ current densities in the winding, the higher values being reached via an active cooling to remove the heat induced by the Joule effect. Superconductivity allows to operate without dissipation of energy, and with ~500 A/mm$^2$, i.e., 100–500 times larger overall current density.

Superconductivity is usually seen as a sustainable technology due to the absence of dissipation, but there is a second aspect that is equally important: 100–500 times larger current densities allow the active part of the magnet to be 100–500 times smaller, inducing a huge saving in the infrastructures, in the quantity of conductor, and in the size of the device.

Only a fraction of the insulated coil (typically 30%) is made of superconductor, the rest being devoted to stabilizer, as quoted in the introduction, to the insulation and to the voids or impregnation between the cable strands. Therefore, accelerator magnets typically operate with 1500 A/mm$^2$ in the superconductor. As it

TABLE I
SET OF PARAMETERS OF SOME SUPERCONDUCTING DEVICES

| | j overall (A/mm$^2$) | j sc (A/mm$^2$) | Ramp rate (mT/s) | Field in sc (T) | T (K) |
|---|---|---|---|---|---|
| Tevatron dipole | 360 | 1550 | ~4 | 4.7 | 4.5 |
| LHC dipole | 360/440 | 1260/1820 | ~8 | 8.6 | 1.9 |
| ATLAS BCT | 30 | 950 | ~0.8 | 3.9 | 4.5 |
| ITER (TF & CS) | 20-40 | 150 | ~400 | 5-13 | 4.5 |
| HL-LHC SC link | 20 | 1450 | ~8 | <1 T | 25 |

will be shown in the next sections, this limit is not strictly due to the properties to the superconductor critical surface: but rather to limitations in mechanics and protection.

### D. Typical Range of Parameters for Main Accelerator Dipoles

Within the class of superconducting devices, main magnets for accelerators have a very challenging set of parameters, as shown in Table I; the overall current density (see Section II–B) is a factor ten larger than in experimental magnets (as ATLAS toroidal coils [10]) or in fusion magnets [11], and in links for power transmission [12]. This large overall current density is needed to keep the global size of the magnet within 0.5 m diameter, thus allowing a compact size of the tunnel (a few meters). Superconducting magnets for accelerators can be seen as the "capsule hotels" of large-scale applications: extremely compact and optimized, to achieve the best ratio between performance, size, reliability and cost. In the Table, we also give the current density in the superconductor $j_{sc}$.

### E. Accelerator Dipole Requirements

Among the superconducting magnets used in particle accelerators, the so-called "cell main magnets" play a special role; they are elements contributing to the beam orbit and linear stability (cell dipoles and cell quadrupoles), and one missing magnet is enough to prevent the beam from circulating.

These magnets have stringent requirements on integrated field / gradient stability and reproducibility (order of 100 ppm relative to operational field) both at the injection plateau, over the ramp and at the high field flattop. This condition becomes very critical at injection, since the ratio injection/flattop field is of the order of 10. For the LHC case, having a ratio 16.6, stability/reproducibility of 100 ppm at injection means that magnets designed for 8 T must be able to operate with a field at 0.5 T reproducible within 0.05 mT, i.e., the Earth's magnetic field. A similar requirement is needed on the field imperfections, that must be controlled within 100 ppm over 2/3 of the bore aperture.

Finally, the ramp must take a negligible time with respect to the duration of a physics run of data taking; since a typical run lasts one day, magnet ramping time should be faster than one hour. This is a quite slow ramp, i.e., order of 10 mT/s compared to pulsed magnets used in injectors, see Table I; but it is a much faster ramp with respect to MRI or HEP experimental solenoids.

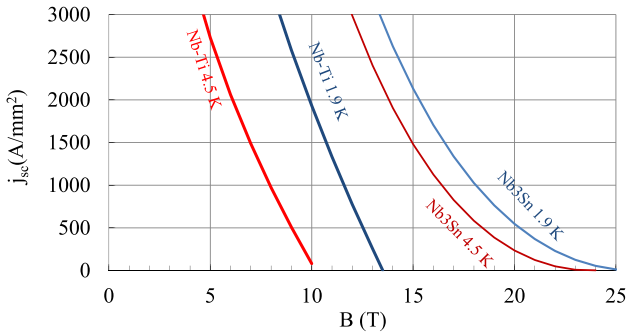


Fig. 2. Critical current surfaces of Nb-Ti and $Nb_3Sn$.

TABLE II
MAIN PARAMETERS OF SOME SUPERCONDUCTING DIPOLES

| | Overall j (A/mm$^2$) | SC j (A/mm$^2$) | Cu j (A/mm$^2$) | Field (T) |
|---|---|---|---|---|
| Tevatron | 360 | 1550 | 835 | 4.4 |
| RHIC | 370 | 1640 | 730 | 3.5 |
| HERA | 288 | 110 | 586 | 5.5 |
| SSC | 320/415 | 1070/1540 | 715/870 | 6.5 |
| LHC | 360/440 | 928/1809 | 760/1254 | 8.3 |

## III. COLLIDERS BASED ON NB-TI: FROM 1970 TO 2010

Here we condense in a few paragraphs the main features of the Nb-Ti technology used in colliders during more than 40 years [13]. As shown in Fig. 2, the mature development of this material can give 1500 A/mm$^2$ of critical current up to 7.5 T at 4.5 K and up to 10 T at 1.9 K.

In the early 1980's Tevatron dipoles achieve 4.3 T operational field: 774 units are made in Fermilab; the design sets a standard for the following 30 years, with the use of high current Rutherford cables (carrying order of 1–10 kA) and collar structure in stainless steel to limit the coil movements during powering via a preload [14].

In the mid 1980's HERA dipoles achieve 4.6 T operational field: 454 dipoles are made in the European industry; the design is based on two-layer coil with wedges and Al collars to reduce the preload loss during cool down [15].

In the 1990's SSC dipole prototypes show ability to operate at 6.6 T; collar material is back to stainless steel, and a grading is introduced in the two-layer coil (higher current density in the outer layer). Even though the project was canceled in 1993, nineteen 17-m-long prototypes are built and successfully tested, plus previous versions with smaller aperture [16].

In the mid 2010's LHC dipoles reach 8.1 T operational field; the design is very similar to the SSC dipoles; this is the first accelerator operated at 1.9 K [17], [18]. Dipole magnetic length goes back to 14.3 m to fit EU regulations for standard transports. Series magnets show the ability of reaching 9.0 T during individual tests. First prototypes date back to the mid 90's.

The main data of these dipoles, also including the "low-cost" dipoles developed for RHIC in the late 90's [19] are summarized in Table II and in Fig. 3: the increase of field from the 3.5 T of RHIC to 8.3 T of LHC is mainly due to the increase of the coil width from 10 to 30 mm, keeping approximately the same

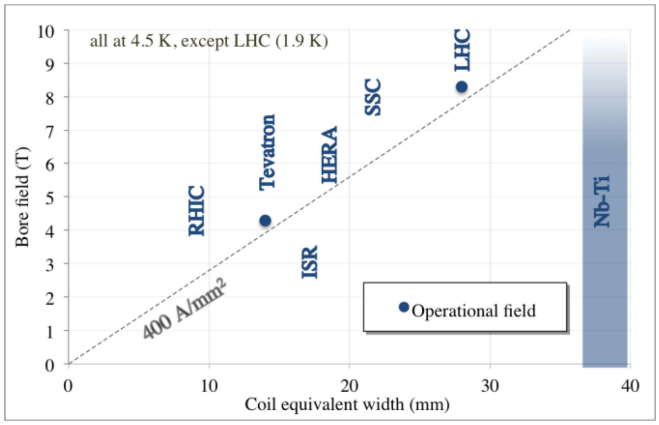


Fig. 3. Operational field versus coil width in main Nb-Ti dipoles used or planned in colliders, and analytical estimate based on $B$[T] = 0.00070 $j$[A/mm$^2$]$w_{eq}$[mm].

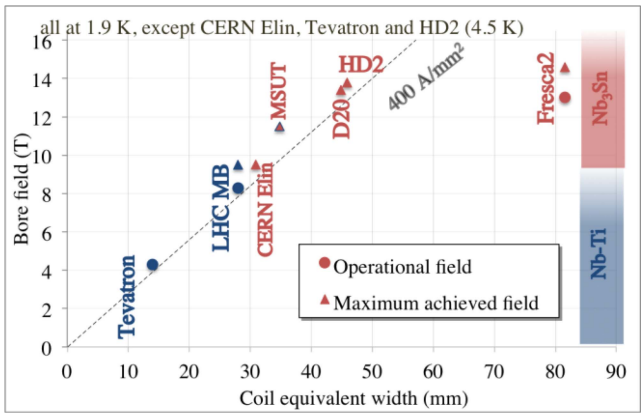


Fig. 4. Operational and achieved field versus coil width in LHC and Tevatron colliders, and in some $Nb_3Sn$ short models.

overall current density of 400 A/mm$^2$ (see Appendix A for the definition of equivalent coil width). In the table we also give the current density in the copper when the superconductor crosses the critical surface: this is a parameter relevant for magnet protection.

## IV. 1989–2010: Short Dipoles Based on $Nb_3Sn$

The limit of maximum achievable field in "affordable" (in the sense of HEP) dipoles based on Nb-Ti is 10 T; LBNL magnet D19 reaches 10.1 T in 1993 [20], MFISC reaches 10.0 T in 1996 [21] and Fresca 10.1 T in 2000 [22]. Adding more coil and lowering the current density one can achieve more field: Iseult Nb-Ti solenoid reaches 11.7 T, but its size is of the order of a few meters [23], [24]. For this reason the concept of ultimate field for Nb-Ti, or $Nb_3Sn$ is ambiguous since it strongly depends on the specific application.

$Nb_3Sn$ opens the way to magnets in the 10-15 T range (see Fig. 2); in the early phases of the LHC design the $Nb_3Sn$ option at 4.5 K is considered [25]. Between the 90's and the 20's several $Nb_3Sn$ dipole models, limited to 1-2 m magnetic lengths, are developed. Here we list the succession of the field records along the years 1989-2015 (see Fig. 4). Other significant magnets such as CERN 11 T or FNAL MDPCT1 are described in the section devoted to developments for 100 TeV colliders.

When comparing the dipoles of the previous section, see Fig. 3, to the $Nb_3Sn$ short models one has to make the distinction between achieved field (maximum field achieved in a reproducible way) given in this section and operational field (maximum field of a sequence of several hundreds or thousands dipoles during beam operation). Just for comparison, the LHC short model dipoles achieve 9.5 T, and half of the series full-size LHC dipoles reach 9.0 T in individual tests, but LHC dipoles operate at 8.1 T.

In 1990 the CERN-Elin dipole reaches 9.5 T at 4.3 K, with a two-layer coil based on cos$\theta$ geometry and grading [25]. This option was not retained for the LHC due to the higher cost with respect to the Nb-Ti option at 1.9 K and to the complexity of the technology.

In the 1990's the MSUT dipole reaches 11.3 T at 4.5 K, with a two-layer coil based on cos$\theta$ geometry and grading [26]. The magnet has been tested again in 2020 at 1.9 K, achieving the power converter limit (11.8 T bore field).

In the 1990's the D20 LBNL dipole reaches 13.4 T at 1.9 K, with a four-layer coil based on cos$\theta$ geometry and strong grading [27], [28].

In the 2000's the HD2 LBNL dipole reaches 13.8 T at 4.5 K, with a novel coil configuration based on a two-layer block design (see Fig. 16). Contrary to previous models, all having an aperture of 50 mm, this magnet has a free bore of 35 mm diameter only [29]. Block design allows to intercept stress accumulation in the midplane via an inner structure.

In the second half of the 2010's, the Fresca2 CERN-CEA dipole reaches 14.6 T at 1.9 K, with a coil configuration based on a four-layer block design. This magnet, conceived as a cable test station operating at 13 T, has a free bore of 100 mm diameter [30], [31], and a very large coil width and low current density: for this reason, it can be considered more a technology demonstrator than an accelerator magnet. Indeed, it has all features conform to accelerator requirements, except for the very large coil width (see Fig. 4) that makes it not affordable.

## V. 2003–2026: The Scaling of $Nb_3Sn$ Technology Up to 7 m in LARP and in the HL-LHC Quadrupoles

### A. Goals of the Project and Magnet Parameters

Six years before the LHC commissioning, i.e., in 2002, works to increase its nominal luminosity are launched, under the name of LHC luminosity upgrade [32]. These studies are later renamed to S-LHC, then to LHC upgrade phase I and II, and then to the HiLumi design study (2010–2013), proposing the final baseline [33], [34] for the High Luminosity LHC (HL-LHC) project, approved in 2014. The goal is very ambitious since LHC luminosity was set to a large value ($10^{34}$ cm$^{-2}$ s$^{-1}$, i.e., 10 times more than the SSC) to be able to compete with the higher energy of the SSC (20 TeV per beam vs the 7 TeV of the LHC).

In 2013, a target of $5\times10^{34}$ cm$^{-2}$ s$^{-1}$ is established for the LHC luminosity upgrade [32], to be achieved via a higher intensity of the proton beam (more fuel) and a twice smaller beam in the Interaction Point (IP), allowing to have four times

more collisions (faster burning). The smaller beam size in the IP makes the beam larger in the triplet quadrupoles, thus requiring larger aperture magnets [34].

After some iterations, outlined in the next section, the quadrupole design aperture has been increased from the 90 mm of first proposals [33] to the 150 mm [34]. $Nb_3Sn$ is selected as magnet technology thanks to the preparatory work done in the US (see next section): 40 years after the ISR interaction region Nb-Ti quadrupoles, a new technology is adopted for accelerators and first used in the collider interaction regions.

The final design adopted for the quadrupole magnet, called MQXF, has an operational gradient of 132 T/m, with $132 \times 0.075 = 9.9$ T pole field and 11.3 T peak field in the coil, thus falling in a field range already explored by previous $Nb_3Sn$ dipole developments described in Section IV. Operational overall current density is 460 A/mm$^2$, with 1300 A/mm$^2$ superconductor current density [35], and a loadline fraction of 0.76; temperature margin is 4.6 K at 1.9 K operation (see Appendix A for definitions of these quantities).

With this gradient, the required length of the four magnets composing the triplet is 7-8 m [36]; the US collaboration, in charge of the construction of these magnets, decides to have two 4.2 m long magnets, not to increase too much the magnetic length already proven by LHC Accelerator R&D Program [37]. Notwithstanding a more limited experience with $Nb_3Sn$ CERN decides to go for the full length of 7.2 m, to open the way to 15-m-long $Nb_3Sn$ dipoles for a future collider, adopting the main features of the LARP design.

A specific challenge of this quadrupole magnet is the accumulation of prestress in the midplane, that can be approximated by [36]

$$\sigma_{\theta\theta}[\rho] = \frac{jGr^2}{4} F_Q(\rho; r). \tag{4}$$

where $\rho$ is the distance to the center of the bore along the midplane, and the shape factor has $F_Q(r,r) = 1$; with the MQXF parameters $jGr^2/4$ is 85 MPa on the inner radius of the coil $\rho = r$, and accounting for the shape factor one finds a maximum accumulation of stress in the midplane (excluding deformation of the structure, and shear stresses) of ~110 MPa [35]. This is very close to the values achieved in a high field dipole with small aperture, where the equation is given by [38]

$$\sigma_{\theta\theta}[\rho] = \frac{jBr}{2} F_D(\rho; r) : \tag{5}$$

with a current density of 400 A/mm$^2$, an aperture radius of 25 mm and a field of 14 T, one finds a stress in the midplane coil at the bore of 70 MPa, that according to (5) can increase inside the coil to ~100 MPa. For the 11 T magnet, also part of the original HL LHC baseline [33] and described in the next section, one has 540 A/mm$^2$, aperture radius of 30 mm, thus giving 90 MPa on the bore. Therefore, MQXF "by chance" has a midplane stress above 100 MPa, the same as a high field dipole for an hadron collider in the 11-14 T range.

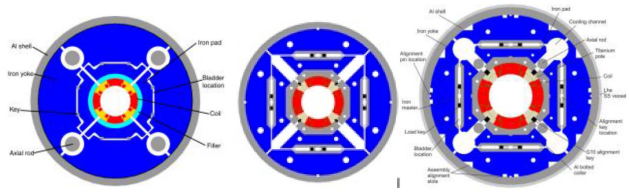

Fig. 5. Cross-sections of TQS, HQ and MQXF.

TABLE III
OPERATIONAL PARAMETERS OF LARP QUADRUPOLES COMPARED TO SOME MAIN DIPOLES

| | Overall j (A/mm$^2$) | SC j (A/mm$^2$) | Cu j (A/mm$^2$) | Peak field (T) |
|---|---|---|---|---|
| Tevatron | 360 | 1550 | 830 | 4.9 |
| LARP TQ | 720 | 2400 | 2100 | 10.0 |
| LARP HQ* | 580 | 1870 | 1650 | 10.3 |
| MQXF | 460 | 1570 | 1310 | 11.3 |
| LHC** | 360/440 | 1250/1810 | 760/930 | 8.7 |

*assuming 172 T/m as nominal gradient
**two values for the LHC correspond to inner/outer layer

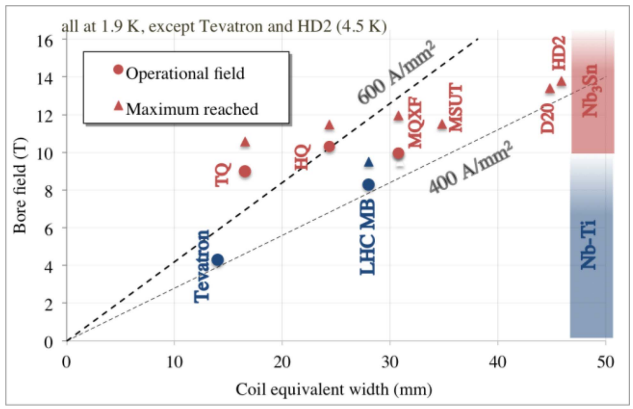


Fig. 6. Operational and achieved field versus coil width in Tevatron, LHC and in some $Nb_3Sn$ short model dipoles, and in LARP/HL-LHC quadrupoles.

### B. LARP Preparatory Phase

In 2004, the US Department of Energy launches a directed R&D to develop $Nb_3Sn$ quadrupoles for the LHC upgrade (LHC Accelerator R&D Program). The goal of the program is the construction of short model quadrupoles TQ with 90 mm aperture and 200 T/m gradient (9.0 T pole field), and the scaling of length up to 4 m [37]. Several models of TQ are built and two structures are explored: a classical one [39] (along the hereditary line of the Tevatron dipoles) based on stainless steel collars and an alternative one based on Al shrinking cylinders and loading via bladder and keys (see Fig. 5) [40], [41]. Both are found to achieve performance, and the latter is chosen, proving better control of mechanics and better performance reproducibility. TQ is a particularly interesting magnet from the point of view of the design, since it operates with a very high overall current density (670 A/mm$^2$, see Table III and Fig. 6); in fact, this magnet is above the limits for quench protection of long magnets to be installed in an accelerator.

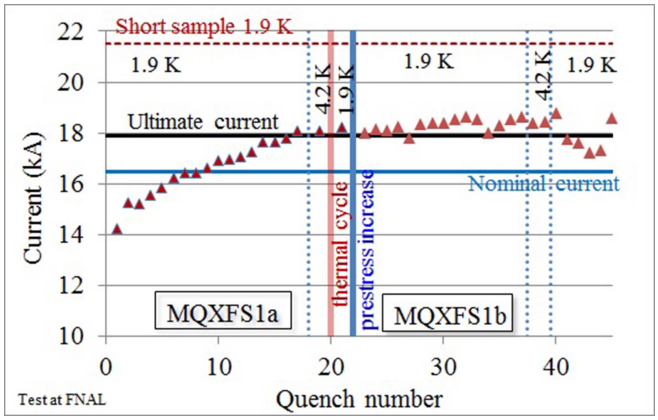


Fig. 7. First powering of first MQXF1 short model.

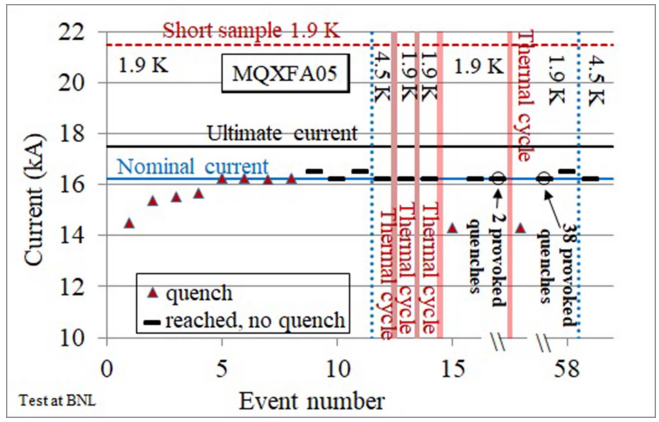


Fig. 8. Endurance test in MQXFA05 [45].

The second phase goes along two directions: an increase of the aperture to 120 mm (HQ [42]), and the scaling in length from 1.5 m to 3.4 m of TQ (LR, and LQ magnets [43]). Both phases require iterations to achieve success: HQ design goes through a fine tuning of the space allocated to the coil during manufacturing, done via a 22 $\mu$m reduction of the strand diameter. It reaches a peak field of 13.35 T at 1.9 K in the second version HQ02. LR shows the need of having in long magnets (above 2 m) segmented Al shells to avoid accumulation of stress due to the different thermal shrinkage between the iron yoke and the aluminum [44]. The LQ magnet reaches 11.1 T peak field (220 T/m gradient), i.e., about 1 T more than the requirements.

It is interesting to note that HQ is presented as a "15 T magnet" [42], referring to the peak field in the coil at short sample limit, and without setting a target for the operational gradient. This confusion between operational peak field, reachable peak field and short sample field can generate misunderstanding with beam dynamics community, and deception for test results: HQ never went to 15 T peak field, but as already said it reached a very honorable 90% of short sample limit (13.3 T peak field), i.e., what was needed to prove the technology.

The third phase starts in 2013 with the selection of the layout for the HL-LHC [34]: it is focused on the MQXF design, in a joint effort between CERN and LARP to build a 150 mm aperture quadrupole operating at 0.80 of loadline fraction [35], and on the construction of several short models. The first magnet is tested in 2016, and has two coils made at CERN and two coils at FNAL. The short model reaches 12.5 T peak field in the coil [44], both at 1.9 K and at 4.5 K, with no need for retraining after thermal cycle to reach the so-called ultimate current (corresponding to the LHC operation at 7.5 TeV, i.e., 7% more than nominal current, see Fig. 7).

### C. MQXF: Reproducibility and Margins

Seven short model magnets are built in 2013-2018, testing a total of 25 coils [36]: six out of seven magnets reach peak field above 13.0 T (i.e., $>$1.5 T more than required operational values). The operational gradient of 132 T/m is also reached at 4.5 K in six out of seven cases, proving that at least 2.6 K of temperature margin is present (out of the 4.6 K by design).

Two prototypes and twelve series magnets out of the twenty required have been built so far in the US and tested vertical at BNL: both prototypes fail to reach performance requirements, and 8 out of 12 series magnets reach the requirements in the first assembly. Among the four series magnets showing performance limitations, three have the limiting coil replaced and then reach the performance requirements [45].

Three prototypes and three series magnets, out of the ten required, have been built at CERN so far: two prototypes failed, but the third prototype and all three series magnets reached performance requirements [46].

Note that both in the US and at CERN the series magnets are powered at 300 A above nominal current at 1.9 K. In addition, the temperature margin is systematically verified at 4.5 K: all magnets are able to operate at nominal current at 4.5 K, with the exception of the first two prototypes of each production.

### D. Endurance

Special attention is given to the performance reproducibility after thermal cycles, powering cycles, and high current quenches. In the initial phase of the production, endurance tests involving more than 5 thermal cycles, more than 100 quenches and more than 1000 powering cycles are performed on two short models and on two full-size magnets (one from the US, see Fig. 8, and one from CERN). In all cases the magnets do not show signs of performance degradation [47].

### E. Impact of Preload

The required preload to maximize performance and to limit training is a highly debated topic in the literature; conservative design requirements are based on no detachment of coil from the pole at 110% of nominal current. On the other hand, it is well known that an unloaded pole does not prevent reaching the corresponding current. For MQXF the strategy is to have a preload to about 90% of electromagnetic forces at nominal current: this allows to have a reliable observable of the pole unloading through strain gauges, thus giving good measure of the coil preload in operational conditions. The pole unloading, visible as a flattening of the stress vs square of the current,

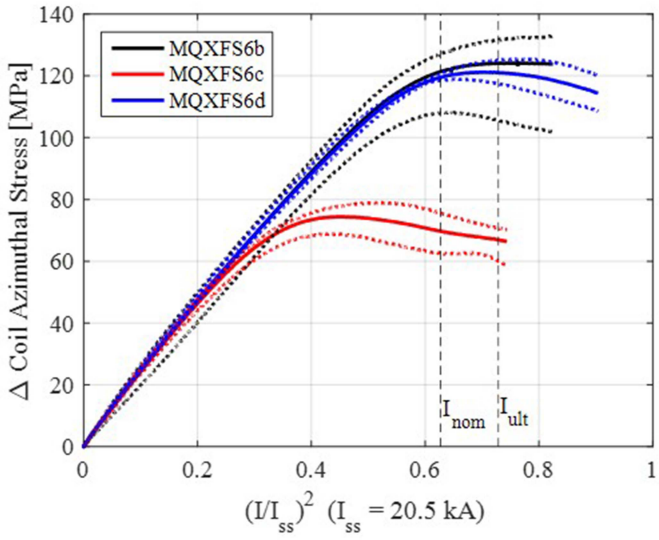


Fig. 9. Pole unloading in MQXFS6 under different preloading conditions (measurements).

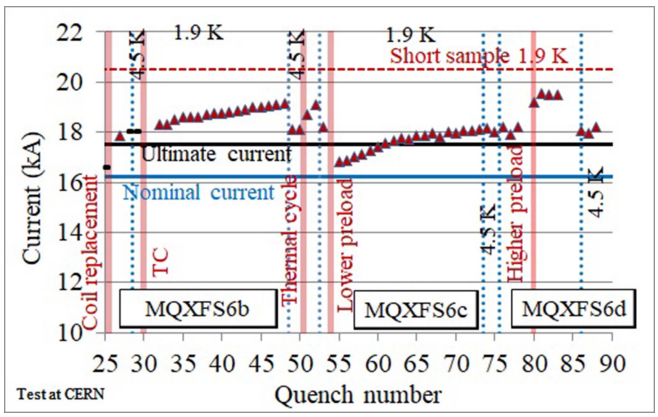


Fig. 10. Nominal preload and low preload in MQXFS6 test.

is needed to have a reliable absolute measurement of stress in cryogenic conditions (see Fig. 9).

The need for full preload and its impact on performance has been measured in a short model MQXFS6, finding that a preload of half what is needed for avoiding pole tension (i.e., 75% of the electromagnetic forces) still allows to reach operational conditions, but prevents from reaching the zone of 90-95% of short sample (see Figs. 9 and 10), and requires a longer training above nominal current [48].

### F. Degradation Due to Stress

Special experiments have been carried out to find the level where stress gives a degradation of performance; irreversible degradation in a PIT conductor used for some short models is visible at 200 MPa, with magnet performance lowered from 100% to 93% of short sample at 4.5 K [49]; in the same magnet the RRP coils did not show signs of degradation up to the level observed in PIT. Note that this value of 200 MPa is an average value based on strain measurements postprocessed via finite element models. This degradation is small, and does not prevent reaching operational values, but is large enough to be clearly measured. A similar experiment to measure this value for the RRP conductor, used in the HL-LHC production, is ongoing.

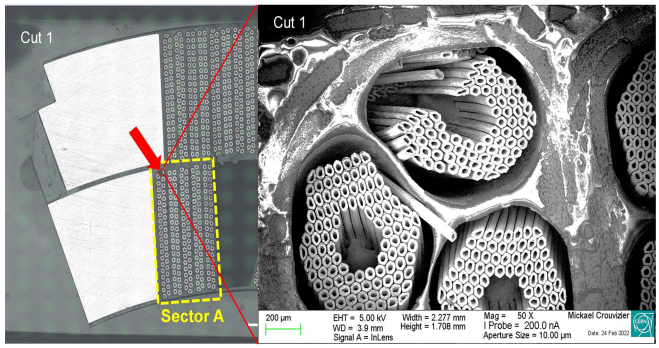


Fig. 11. Broken filaments in first MQXFB prototype.

### G. Overcoming Performance Limitations

Understanding the cause of a magnet performance limitation is a difficult task. The concept itself of limitation is vague, since it depends on the requirements, since one could state that any magnet not reaching short sample condition is performance limited. On the other hand, for the accelerator operators whatever reaches requirements is not performance limited. In our opinion, a magnet reaching more than 90% of short sample limit can be assessed as without major performance limitations, even though we are aware that not all the colleagues will agree with this definition.

Main MQXF requirements are (i) reaching nominal current at 1.9 K with 300 A margin, and (ii) ability to hold nominal current for several hours. Among the magnets not reaching these requirements we see two main classes: four US MQXFA magnets out of a total of 15 [45], that show along the production the presence of limiting quenches in specific coils heads, generally believed to be local concentration of axial stress due to non-optimal preload. In all cases the limiting coil has been replaced, and the magnet has reached the performance. The second case is seen in first two CERN MQXFB prototypes and first two series magnets, showing a very reproducible limit in the central part of the magnet, due to a manufacturing issue in the coils. This limitation has been solved by removing the binder from the outer layer. In both cases, a metallographic analysis showed the massive presence of broken filaments [50], [51], thus connecting the performance limitation to a visible defect (see Fig. 11for MQXFB).

The US program also had two prototypes not reaching performance: the first one after reaching target current lost electrical integrity during a quench, due to a non conforming component in the coil manufacturing. The second one had an Al shell broken due to the presence of sharp corners in the structure, that were removed in the following ones.

It is rather striking that all magnets showing performance limitation are able to reach 14 kA, i.e., nearly 10 T peak field:

TABLE IV
THE EVOLUTION OF THE FCC-HH MAIN PARAMETERS

| | | CDR 2019 | 2024-$Nb_3Sn$ | 2024-HTS |
|---|---|---|---|---|
| Dipole field | (T) | 16 | 14 | 16/20 |
| Tunnel length | (km) | 100 | 90.7 | 90.7 |
| Arc length | (km) | 82.0 | 76.9 | 76.9 |
| Arc filling factor | (adim) | 0.80 | 0.83 | 0.86 |
| Energy c.o.m. | (TeV) | 50+50 | 42.5+42.5 | 50+50/62+62 |
| Loadline fraction | (adim) | 0.86 | 0.80 | TBD |
| $j_c$ at 16 T 4.2 K | (A/mm$^2$) | 1500 | 1200 | TBD |

all the battle for performance takes place in the range between 70% and 80% of short sample. 15 years ago, before starting HL-LHC project, nobody would have bet to have more than 20 magnets of a new technology, all reaching 70% of short sample. But, obviously, 70% is not enough for us.

### E. Novel Paradigm for Protection: CLIQ

The HL-LHC magnets are characterized by a large energy density on the coil (i.e., the ratio between the stored energy and the volume of the insulated coil, that absorbs the energy during a quench), and a limited amount of copper: just for comparison, in MQXF the energy density on the coil is 0.10 J/mm$^3$ compared to 0.05 J/mm$^3$ in the LHC dipole. Moreover, the fraction of copper is 1.2 compared to 1.65/1.95 in the LHC dipole [36]. In the first baseline, it was found that quench heaters on the outer layer, i.e., the protection baseline for the LHC dipoles, were not enough to guarantee adequate protection, including failure cases. Therefore, they were complemented by inner layer quench heaters, glued on the inner surface of the coil towards the bore tube. Even though these heaters proved to be effective to rapidly quench also the inner layer, they showed detachment after firing. Moreover, polyimide constitutes a barrier to one of the major paths to magnet cooling; after several attempts they were abandoned.

Inner layer quench heaters were replaced by a novel system, called CLIQ (coupled losses induced quench) [52], [53], sending a impulse of current of the order of 1 kA in the middle of the coil to produce heating via coupling losses. This system proved to be a perfect complement to outer layer quench heaters, and provides a hotspot temperature in nominal cases below 270 K. It is now currently used during magnet test, not only of MQXFA but also of many others in different labs. CLIQ is the baseline for the HL-LHC, it will be tested in the full circuit including four MQXF magnets in the string facility, that is being completed at CERN [54].

## VI. 2010 TO PRESENT: R&D ON $Nb_3Sn$ DIPOLES FOR 100 TEV COLLIDERS

### A. Requirements for FCC-hh

In 2014, the studies for a Future Circular Collider at CERN are launched. First baseline aims at a seven-fold increase of LHC energy thanks to a 2 times larger field and 3.5 larger curvature radius, corresponding to a 100 km circumference tunnel (see Table IV [55]). In 2024, the tunnel size is revised to 91 km, and the field is lowered to 14 T to better fit the $Nb_3Sn$ technology, resulting in a 85 TeV c.o.m energy thanks to an increase in the filling factor. The reduction of the operational field to 14 T allows also to increase the loadline margin to 20%, as in the HL-LHC quadrupoles, using the existing $Nb_3Sn$ high performance strand. The present baseline is at 1.9 K, but the HL-LHC results could open the possibility of operating magnets built for 20% loadline margin at 1.9 K also at 4.5 K, with some saving in the operational costs and in the cryogenic system. An HTS version is also considered, with 20 T dipoles and c.o.m. energy up $\sim$120 TeV.

TABLE V
THE EVOLUTION OF THE SPPC MAIN PARAMETERS

| | | phaseI: $Nb_3Sn$ (2019) | phaseII: HTS (2019) | $Nb_3Sn$/HTS (2023) |
|---|---|---|---|---|
| Dipole field | (T) | 12 | 20/24 | 13+7 |
| Tunnel length | (km) | 100 | 100 | 100 |
| Arc length | (km) | 81.8 | 81.8 | 81.8 |
| Arc filling factor | (adim) | 0.79 | 0.79 | 0.79 |
| Energy | (TeV) | 37.5+37.5 | 60+60/75+75 | 62.5+62.5 |

### B. Requirements for SPPC

A few years after the beginning of the activities for FCC, studies for a circular collider of 100 km length are launched in China: a version for leptons, named CepC, and a version for hadrons, named SppC [56]. The first set of parameters for the hadron collider is based on a two-phase approach: first a 75 TeV energy c.o.m. based on $Nb_3Sn$ 12 T dipoles, and then a 125-150 TeV version with 20-24 T magnets based on HTS. This baseline is updated in 2023, with a single-phase based on 20 T magnets, 13 T being provided by $Nb_3Sn$ and the additional boost of 7 T by HTS (see Table V). Operational temperature is 4.5 K.

### C. Conductor Needs

For the LHC dipoles the total need of conductor at short sample field is 67 GA.m (54 MA.m for each of the 1232 magnets, see Fig. 12); for the 100 TeV colliders presented in the previous sections, one needs one order of magnitude more. In the hypothesis of having a 400 A/mm$^2$ overall current density in the insulated winding, and 20% margin on the loadline, the requirement in terms of ampere-turns meters is 0.5 TA.m for the 14 T FCC-hh accelerator at 90 TeV, and twice that for a 125 TeV collider. This means having a 1 kA cable long as 1.5 to 3 times the distance from the Earth to the Moon. This is a huge opportunity for the industrial suppliers, with orders of 2500-5000 M$ (using the target price of 5 $/kA m given for EuroCirCol studies [57], [58]).

### D. Cosθ Coils: 11 T, MDPCT1 and Future Plans

Besides the interaction region magnets, the HL-LHC project also had a $Nb_3Sn$ 11 T dipole [59] to replace a standard LHC dipole in a few locations of the accelerator (initially 8, then 2),

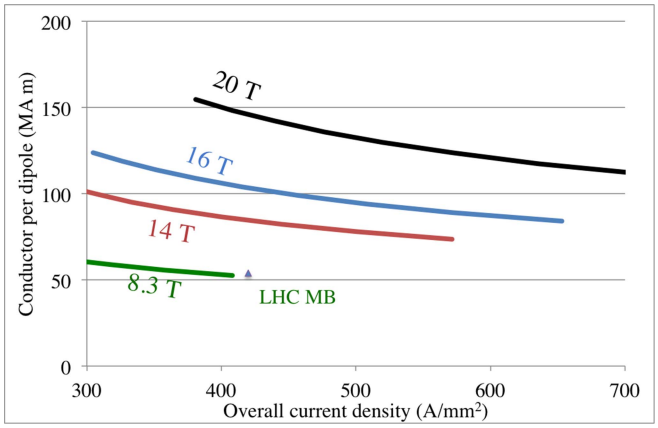


Fig. 12. Ampere turn meters needed for a 50 mm aperture magnet, 14.3 m magnetic length, at different field levels, vs overall current density; analytical curves based on sector model and real designs.

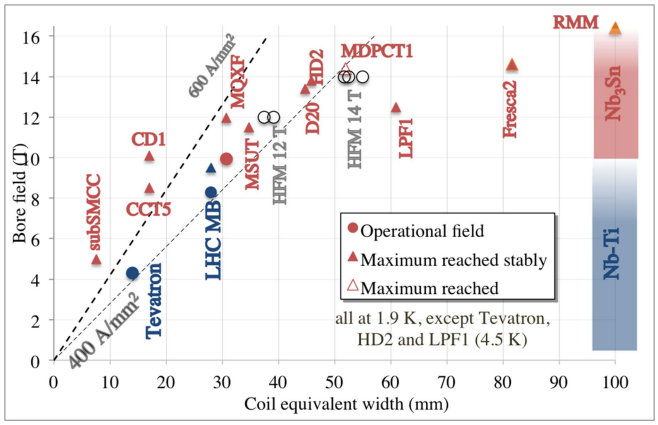


Fig. 13. Operational and achieved field versus coil width in Tevatron, LHC and in some $Nb_3Sn$ dipole models.

making space for collimators. Note that the increase in the field from 8.3 T to 11 T is obtained by a coil with the same width and higher current density compared to the LHC dipole (540 A/mm$^2$ rather than 360/440 A/mm$^2$), see Fig. 13. The 11 T short model program shows ability of reach the field target, but with a limited reproducibility (6 out of 9 successful models [60]) and the extension to 5-m-long magnets shows a loss of performance after thermal cycle in several cases. The program is canceled in 2020 but achieves two significant results: (i) the first double aperture $Nb_3Sn$ dipole magnet, fully compatible with machine operation and (ii) the first scaling of $Nb_3Sn$ to 5-m lengths, reaching more than 11 T bore field.

Initially the program is a collaboration between FNAL and CERN; in FNAL two single aperture short models are built [61] and the coil manufacturing technology is transferred to CERN. On the other hand, the synergy between the two programs is limited, as FNAL and CERN use different mechanical structures. Length scaling is done at CERN only.

In 2020, in FNAL the 11 T coils are used as an inner double layer for a four-layer cos$\theta$ magnet, with grading between the inner two layers and the outer two layers, for a total coil width of the order of 50 mm, named MDPCT1. The magnet reaches 14.5 T at 1.9 K and has been the first magnet to go above 14 T at 4.5 K [62]. After reassembly the performance degrades after a thermal cycle by more than 10% [63]: in FNAL this development line is abandoned for a stress managed cos$\theta$ design, see Section VI.H. Plans for building cos$\theta$ magnets for FCC are ongoing at CERN and in INFN, with a 12 T double layer and a 14 T four layer coil [64], [65].

### *E. Block Designs: RMM Demonstrator, and Future Plans*

During the EuroCirCol program [57] CERN developed a technology demonstrator to prove the ability of $Nb_3Sn$ to reach the 16 T target; to achieve this high field, a 50 mm aperture magnet [66] was built with an extremely large coil width (order of 100 mm), able to provide the required field with a very low current density (250 A/mm$^2$). The magnet, called RMM, reached 16.4 T in the first assembly [67] and 17 T in the second one. However, it had flattop quenches in the range 16-17 T, but it was able to hold 15.75 T for several hours. This confirms the soundness of 14 T as operational field for FCC-hh based on $Nb_3Sn$. This magnet does not have flared ends, but the straight section is representative of a block coil. A third assembly with a new set of coils will be made in early 2025.

CERN is developing a double aperture magnet (BOND) based on a block design with a 55 mm coil width to reach 14 T without grading at 330 A/mm$^2$ overall current density [68]. CEA is also developing a single aperture magnet (F2D2) with grading and external splices [69].

### *F. Common Coil Designs: LFP1, and Future Plans*

The common coil design is an intrinsically double aperture magnet, based on racetrack coils plus non-planar correction coils; the idea has been proposed in the 90's [70], and is today the design that has been adopted for the SppC dipole. In 2022, IHEP built as technology demonstrator an hybrid $Nb_3Sn$/Nb-Ti magnet called LFP1-U that reached 12.5 T in two small 14-mm-diameter apertures [71], and 90% of short sample at 4.5 K (see Fig. 13). Next step is LFP3, aiming at 13 T obtained via $Nb_3Sn$ plus 3 T via HTS [72].

The common coil path is being followed also by CIEMAT in the HFM program, aiming at a 14 T operational field with $Nb_3Sn$, based on a common coil design in a 50 mm aperture. CIEMAT program, as IHEP, has a step-by-step approach, with as technology demonstrator a first assembly of RMM coils provided by CERN in a common coil configuration, with a 35 mm aperture and targeting a field of 13 T [73]. As LFP1-U, this magnet will not have the corrective coils and therefore neither the field quality nor the aperture of these common coils is adapted to the collider requirements yet.

### *G. What Happens Around 15 T?*

Around 15 T operational field a "new physics" appears for the magnet designers due to three limitations: superconductor properties, mechanics and protection. A 15 T operational field magnet requires a 18.5 T short sample field (assuming 0.80 loadline fraction), and at this field level $Nb_3Sn$ current density is

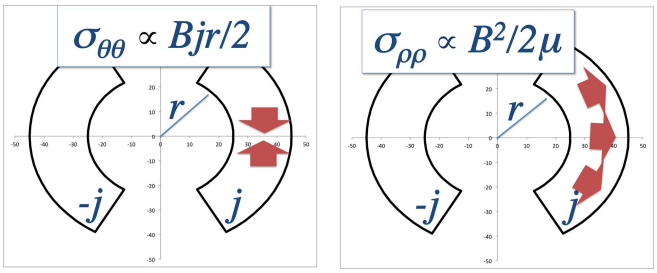


Fig. 14. The two components of stress induced by electromagnetic forces in a cos$\theta$ coil.

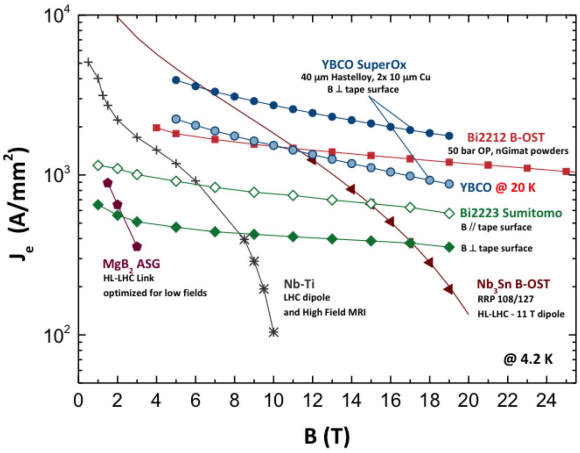


Fig. 15. Critical current surfaces of HTS, $Nb_3Sn$ and Nb-Ti, engineering current density (courtesy of A. Ballarino [58], and P. Lee [82]).

far below the 1000 A/mm$^2$ required to have an efficient magnet (see Fig. 2): this is the first limitation.

A second limitation is related to mechanics, and in particular to strain induced in the winding by electromagnetic forces. The stress induced by electromagnetic forces in a thin cos$\theta$ coil scales in two different ways for radial or azimuthal stress [74] (see Fig. 14): radial stress is proportional to magnetic pressure (it can be 50% larger due to the asymmetry of the field). Azimuthal stress scales with aperture field and current density as shown in (5). Assuming a 50 mm bore diameter, and a 400 A/mm$^2$ overall current density, at 15 T the contribution given by magnetic pressure becomes as important as the azimuthal prestress and becomes overwhelming at larger fields (see Table IV). Therefore, at ~15 T one has to care about not only azimuthal stress, that is the concern for design based on cos$\theta$ configurations, but also radial stress.

Since the scaling laws shown in Fig. 14 have additional shape factors that increase them by about 50%, at 15 T one approaches the 120 MPa level both in azimuthal and in radial stress induced by the e.m. forces. Note that on the top of this, you have to add the structure loading, coil deformations, reaching a value of 150 MPa (in simulations), which is generally known as a conservative range for the beginning of degradation for $Nb_3Sn$.

The third limit is due to protection. Magnetic field is pressure, or equivalently, energy density. 100 MPa of pressure correspond to 0.1 J/mm$^3$. The enthalpy of a coil from 2 K to 300 K is ~0.5 J/mm$^3$. Since the stored energy of the magnetic field has

TABLE VI
MAGNETIC FIELD PRESSURE, ENERGY DENSITY AND ENERGY DENSITY ON THE COIL FOR 50 MM APERTURE AND 400 A/MM$^2$ CURRENT DENSITY

| | $B^2/2\mu_0$ (MPa) | $Bjr/2$ (MPa) | $B^2/2\mu_0$ (J/mm$^3$) | *Coil energy density* (J/mm$^3$) |
|---|---|---|---|---|
| 4 T | 6 | 20 | 0.006 | 0.017 |
| 8 T | 25 | 40 | 0.025 | 0.046 |
| 11 T | 48 | 55 | 0.048 | 0.075 |
| 14 T | 78 | 70 | 0.078 | 0.110 |
| 16 T | 102 | 80 | 0.100 | 0.140 |
| 20 T | 159 | 100 | 0.160 | 0.200 |

to be dumped in the coil, the energy density of the coil (i.e., the stored energy divided by the volume of the coil) must be far away from the enthalpic limit. In Table VI we also give an estimate of the energy density in the coil, for a 50 mm aperture and 400 A/mm$^2$ current density. Note that LHC magnets had a 0.05 J/mm$^3$ energy density, and HL-LHC magnets are at 0.10 J/mm$^3$. A value of 0.15 J/mm$^3$ appears to be above the limits of the present protection systems. Therefore, above 15 T one also hits the protection limit, i.e., the coil has not enough enthalpy to absorb the magnet stored energy, including the time needed to detect the quench and to make the protection system effective. All these aspects require new paradigms for magnet design, that will be described in the next section.

### *H. Stress Managed Magnets: cosθ, CCT and Future Plans*

A stress managed magnet [75] can be defined as a design where the supporting structure is not only external (as in the cos$\theta$ layout) or external and internal (as in the block design), but it is also spread within the coil. The advantage is twofold: (i) the structure can intercept forces and avoid stress accumulation and (ii) the structure can participate to absorb the energy in case of quench. This can allow using much higher current densities, and then to build more efficient magnets (i.e., using less conductor). The disadvantage is that one cannot preload the coil, and therefore training can become very long.

The stress-managed structures are probably the only way to go above 15 T operational fields. US-MDP research program is strongly investing in this direction [76], [77], [78], proposing two designs both based on stress management. A stress managed cos$\theta$, where a cos$\theta$ coil is wound on a former that includes the wedges, is being studied in FNAL. A $Nb_3Sn$ coil in mirror configuration has reached 12.7 T at 87% of short sample limit [78].

A fully stressed managed magnet is the CCT (canted cos$\theta$) configuration, where each turn is supported by a rib integrated to a former. This design, also called tilted solenoid or double helix, dates back to the early 70's [79] and has been adopted by LBNL since mid of the 00's to reach fields towards 20 T [80]. The main additional drawback with respect to the previous option is that the use of conductor is less optimized, since part of it is used to generate a solenoidal field that is canceled by the other coil. However, the structure is totally mixed with coil – a kind of endoskeleton - making easier protection and mechanics and possibly allowing higher current densities; therefore, in absence

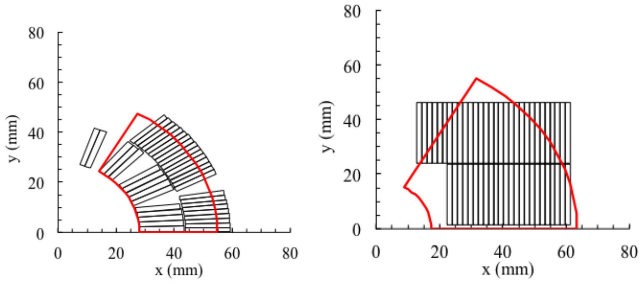


Fig. 16. Coil layout for the LHC and for the HD2 dipole, and equivalent coil width (width of the red sector).

of limitations due to superconducting properties, magnets based on this design could be cheaper.

The short model CCT5 built in LBNL reached 8.5 T with a $Nb_3Sn$ winding using a 10 mm cable over a 90 mm aperture [80]. In PSI, using a similar design and the same cable, 10.1 T were reached in a 60 mm aperture short model named CD1 [81]. Overall current densities (over the insulated coil) are in both cases extremely large (800 and 1000 A/mm$^2$ respectively): a field of 8-10 T is reached with a coil width of the order of 17 mm (see Fig. 13). Recently, PSI abandoned the CCT design to go for a common coil with stress management [81], whereas LBNL is pursuing this path both for $Nb_3Sn$ and for HTS [77].

## VII. HTS Perspectives

### A. HTS: The Ideal Superconductor

An ideal superconductor would have a flat critical surface, i.e., independent of the field, giving >2000 A/mm$^2$ well above $LN_2$ temperature: flat means that the magnetic field is not limited by superconductivity, 2000 A/mm$^2$ means that magnets have enough margin and are efficient, and $LN_2$ means cheap cryogenics. Moreover, avoiding the "natural" increase of critical current with decreasing fields reduces hysteresis losses and field imperfections. Finally, the superconductor should be available in fine filaments, be cheap (order of 5 $/kA m), and tolerant to stresses at least up to 200 MPa.

HTS, discovered in the mid 80's, appear quite close to these requirements for the shape of the critical surface and for the ability of maintaining superconductivity at temperatures well above 20 K (see Fig. 16), even though the Holy Grail would be to operate in liquid nitrogen. On the other hand, HTS are still far from having the fine filaments required for HEP applications, and the most popular conductor come in tapes, ideal for solenoids or flat coils needed for fusion, but not for dipoles.

Three types of superconductors are available today. BSSCO [83], mainly developed in the US, has the advantage of being available in round strands, but it is very expensive. Manufacturing is complex since it needs as $Nb_3Sn$ a reaction after winding, but at 900 C. Some short models were successfully done (see next subsection).

The second one is REBCO [84]; this conductor is available only in tape, and its development is profiting of a B$ private investment aiming at ultra-compact tokamak with 20 T poloidal coils. This has brought the price at 4.5 K not so far from $Nb_3Sn$ at 1.9 K (comparison is nontrivial since it depends on requirements and margins). The conductor is already reacted and therefore the manufacturing of coils is not as complex as $Nb_3Sn$ or BSSCO. On the other hand, unit lengths are still problematic and affect the cost. REBCO is a strongly anisotropic conductor, and the challenge is not only to make a cable from a tape, but also to control hysteresis losses as filaments are very large in one direction.

The third one is the family of the iron-based superconductors [85], [86]: it is being strongly pursued in China. Critical current density is still lagging a factor 2-3 behind the expectations given 10 years ago, but the material has the potential of a very low cost: this can be a significant advantage for a collider magnet where at least half of the price is the superconductor.

### B. Achieved Fields in Eucard2 and MDP Dipole Models

Between 2015 and 2020, three dipole magnets based on REBCO are built within the framework of Eucard2 program [87]. In CEA, a dipole technology demonstrator based on double REBCO ribbons and three racetrack coils, without aperture, reaches 5.4 T [88]. In the same period, two magnets are built with Roebel cable: in CEA a 40 mm aperture dipole is manufactured with a cos$\theta$ configuration, 12 mm coil width, reaching 1.16 T due to one degraded coil [89]. At CERN a dipole is built with the same cable, with an aligned block dipole configuration in a 40 mm aperture, reaching 3.35 T at 5 K and 4.3 T at 4.5 K (FeatherM2.12 and 2.34 [90], [91]).

More recently, the US program MDP develops a CCT magnet with Bi2212 (Bin5) reaching 1.6 T in a 31 mm aperture [92]. And a CCT with a CORC cable based on a REBCO tape reaches 2.9 T in a 65 mm aperture [93].

### C. Plans for 20 T

The Eucard2 program was based on having a HTS insert in a $Nb_3Sn$ external coil [87]; the same design is being now adopted by US-MDP and IHEP. MDP proposes to achieve 20 T via a magnet using different designs [78]: a CCT for the HTS part, and stress managed cos$\theta$ for the inner $Nb_3Sn$ layer and a classical cos$\theta$ for the outer layer. IHEP common coil design is also based on an HTS inner coil and $Nb_3Sn$ outer coils [73], with HTS contributing 5 T to the field.

The hybrid option HTS/$Nb_3Sn$ prevents from profiting of the higher operational temperature that would be possible with a full-HTS magnet (possibly 20 K). For the moment $Nb_3Sn$ is still cheaper/better mastered than HTS, and therefore both US and China work on the hybrid option, at least to make technology demonstrators. It must be noted that the cost per kA m for HTS at 20 K is three times larger than at 4.5 K, and since the conductor is the driving parameter of the magnet cost, this can be a showstopper for the 20 K option.

### D. Challenges: Field Reproducibility and Insulation, Stress, Hysteresis Losses, Protection

A stringent requirement for accelerator main magnets is the precision and reproducibility in the transfer function not only at high field, but also at injection and during the ramp. This aspect is strongly related also to the design of insulation and protection: HTS coils that are being made for fusion, having to work at fixed field, make use of non-insulated coil, allowing current redistribution that eases reaching higher fields and protection. This option is not suitable for accelerator magnets, which require a dielectric insulation. Metal insulations are also being studied, allowing a better control of the interturn insulation, but they are not yet proven to be suitable for accelerator magnets.

Another issue is related to stress in the winding, that causes delamination of the superconductor layer from the supporting substrate, degrading the cable performance.

The high temperature margins of HTS have the drawback that quench velocities are slow, and the build up of voltage to detect the quench can take too long. Moreover, at 20 T the energy density to be absorbed by the coil is well above the enthalpic limit: protection of HTS coils is still a major challenge, and coils that reached 20 T for fusion applications were lost during quenches. Systems that can provide a partial extraction of the stored energy for long magnets are being studied. Another possibility would be to avoid quenches, i.e., having a system that, once the resistive transition is seen, manages to prevent the thermal runaway.

Finally, since the current density at low fields is much smaller than in LTS, and the temperature margin is much larger, stability can be achieved by very large filaments (see (1)): tapes used for fusion have a width of 4 to 12 mm, and this produces a very large magnetization, giving rise to hysteresis losses that are one order of magnitude larger than LTS. This effect can be a bottleneck for HEP applications.

## VII. Summary and Conclusion

In this paper we outlined the specific features of superconducting accelerator magnets: (i) operating at very high overall current densities, (ii) requiring field reproducibility and control over a large range and not only at a specific current, and (iii) having severe constraints in terms of size and cost.

We then reviewed the evolution of application of Nb-Ti to main dipoles in colliders, showing how the field increase from 3 T (RHIC) to 8 T (LHC) has been given by larger coil width and similar current densities of ∼400 A/mm$^2$. Short models in $Nb_3Sn$ followed the same path, reaching values in the 10-14 T range and coil width from 30 to 50 mm. HL-LHC $Nb_3Sn$ quadrupoles are proving the first scaling in length from 1 to 7 m: we outlined the main results and challenges of this mini-series of 30 magnets, the first to be installed in a collider. We then outline the present status of the R&D towards magnets operating at 14 T for 100 TeV colliders in Europe and in China. Above 15 T, limitations appear in mechanics and protection that require new concepts in magnet design, namely stress managed coils. These designs could also allow to use a much higher current density, thus providing cheaper magnets for the 14 T applications.

HTS opens a brave new world, with superconductors tolerating fields up to 50 T, large temperature margins and decreasing costs thanks to massive investments of fusion community. Their use for accelerator main magnets is still to be proven, and until now technology demonstrators in the 1-5 T range built in the past 10 years have not been conclusive: we outlined the main opportunities and challenges of this technology.

We wish to acknowledge A. Yamamoto, Q. Xu, T. Salmi, L. Rossi, A. Milanese, A. Ballarino, S. Izquierdo Bermudez, H. Felice, H. ten Kate, B. Strauss, L. Chiesa, P. Ferracin and S. Prestemon for feedback and comments on this plenary talk. This work has been partially supported by High Field Magnet (HFM) program.

## Appendix

### A. Equivalent Coil Width, Current Densities

The equivalent coil width is a concept used to measure the quantity of insulated conductor. Rather than using the coil cross-sectional surface $A$, we define the equivalent coil width $w_{eq}$ as the width of the 60° sector whose coil surface is the same (see Fig. 16)

$$A = \frac{2\pi}{3}\left[(r+w_{eq})^2 - r^2\right] \Rightarrow w_{eq} \equiv r\left(\sqrt{\frac{3A}{2\pi r^2}+1}-1\right).$$

Note that in the definition of surface $A$ we include voids and insulation in the cables but not the wedges. This definition provides a variable related to the quantity of conductor that is related to the field and to the overall current density via

$$B = \gamma_c j w_{eq}.$$

### B. How to Include Quadrupoles in the Plots Field Vs Coil Width

The equation for the quadrupole in the case of a 30° sector is

$$G = \gamma_c j \ln\left(1+\frac{w}{r}\right),$$

and therefore for the pole field $B_q$ we have

$$B_q \equiv Gr = \gamma_c j r \ln\left(1+\frac{w}{r}\right).$$

To add the quadrupoles in the plots of Figs. 3, 4 and 11 (dipole bore field vs equivalent coil width) we use the pole field $B_q$ and the quantity $r\ln(1+w_{eq}/r)$.

### C. Loadline, Current and Temperature Margin

For superconducting magnets, one usually defines the short sample conditions as the combination of superconductor current density, peak field in the coil, and operational temperature that lays on the critical surface (see Fig. 17). One operates the magnet at a fraction of this value (called loadline fraction), typically in the 75-85% range for main magnets.

The current margin is the ratio between the operational current and the maximum current on the critical surface at operational field and temperature (see Fig. 17).

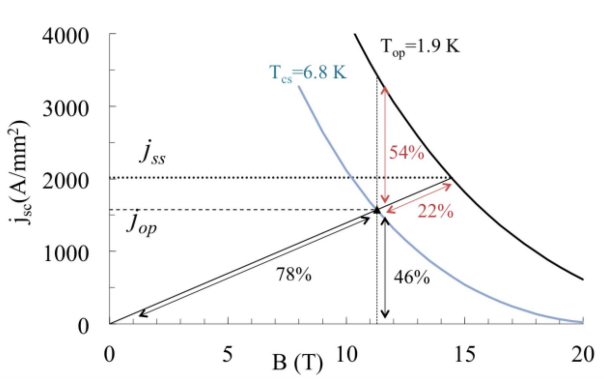


Fig. 17. Loadline margin of 22%, current margin of 54%, temperature margin of 4.9 K for a magnet operating at 11.3 T peak field, 1550 A/mm$^2$ $Nb_3Sn$ superconductor current density.

The operational current density in the superconductor and the corresponding peak field are on the critical surface for a given value of the temperature (called current sharing temperature $T_{cs}$). The difference between this temperature and the operational temperature is the temperature margin. The case of margins for HL LHC triplet is shown in Fig. 17.

## REFERENCES


[1] M. N. Wilson, "100 Years of superconductivity and 50 years of superconducting magnets," *IEEE Trans. Appl. Supercond.*, vol. 22, no. 3, Jun. 2012, Art. no. 3800212.

[2] A. Wood, *Magnetic Venture: The Story of Oxford Instruments London*. London, U.K.: Oxford Univ. Press, 2001.

[3] H. T. Coffey et al., "A protected 100-kG superconducting magnet," *J. Appl. Phys.*, vol. 36, pp. 128–136, 1965.

[4] G. Hamilton, "The man with the golden gun," United Artists, 1974.

[5] J. Billan et al., "The eight superconducting quadrupoles for the ISR high-luminosity insertion," in *11th International Conference on High-Energy Accelerators* (Series Experientia Supplementum), vol. 40. Berlin, Germany: Springer, 1980, pp. 848–852.

[6] P. Lebrun, S. Pichler, T. M. Taylor, T. Tortschanoff, and L. Walckiers, "Design, test and performance of the prototype superconducting quadrupole for the LEP low-beta insertions," *IEEE Trans. Magn.*, vol. 24, no. 2, pp. 1361–1364, Mar. 1988.

[7] T. M. Taylor, T. Tortschanoff, G. Trinquart, and L. R. Williams, "Design of the superconducting quadrupoles for the LEP200 low-beta insertions," *IEEE Trans. Magn.*, vol. 28, no. 1, pp. 382–385, Jan. 1992.

[8] A. Ijspeert et al., "Construction and tests of a model of the LHC superconducting corrector magnet MDSBV," *IEEE Trans. Magn.*, vol. 28, no. 1, pp. 354–357, Jan. 1992.

[9] E. Todesco and M. Giovannozzi, "Optimizing the filling factor in high energy colliders," in *Proc. Int. Part. Accel. Conf.*, 2023, pp. 3709–3711, doi: 10.18429/JACoW-IPAC2023-WEPM061.

[10] H. H. J. Kate, "ATLAS superconducting toroids and solenoid," *IEEE Trans. Appl. Supercond.*, vol. 15, no. 2, pp. 1267–1270, Jun. 2005.

[11] N. Mitchell et al., "The ITER magnet system," *IEEE Trans. Appl. Supercond.*, vol. 18, no. 2, pp. 435–440, Jun. 2008.

[12] A. Ballarino, "Alternative design concepts for multi-circuit HTS link systems," *IEEE Trans. Appl. Supercond.*, vol. 21, no. 3, pp. 980–983, Jun. 2011.

[13] A. Tollestrup and E. Todesco, "The development of superconducting magnets for use in particle accelerators: From the Tevatron to the LHC," *Rev. Accel. Sci. Technol.*, vol. 1, no. 1, pp. 185–210, 2008.

[14] R. Hanft et al., "Magnetic field properties of Fermilab energy saver dipoles," *IEEE Trans. Nucl. Sci.*, vol. TNS-30, no. 4, pp. 3381–3383, Aug. 1983.

[15] R. Meinke, "Superconducting magnet system for HERA," *IEEE Trans. Appl. Supercond.*, vol. 27, no. 2, pp. 1728–1734, Mar. 1991.

[16] J. Strait et al., "Tests of full scale SSC R&D dipole magnets," *IEEE Trans. Magn.*, vol. 25, no. 2, pp. 1455–1458, Mar. 1989.

[17] R. Perin, *Encyclopedia of Applied Superconductivity*. London, U.K.: IOP, 1998.

[18] L. Rossi, "The LHC main dipoles and quadrupoles toward series production," *IEEE Trans. Appl. Supercond.*, vol. 13, no. 2, pp. 1221–1228, Jul. 2003.

[19] M. Anerella et al., "The RHIC magnet system," *Nucl. Instrum. Methods Phys. Res. Sect. A: Accelerators, Spectrometers, Detectors Assoc. Equip.*, vol. 499, no. 2/3, pp. 280–315, Mar. 2003.

[20] D. Dell'Orco et al., "A 50 mm bore superconducting dipole with a unique iron yoke structure," *IEEE Trans. Appl. Supercond.*, vol. 3, no. 1, pp. 637–641, Mar. 1993.

[21] J. Ahlback et al., "Construction of a 56 mm aperture high-field twin-aperture superconducting dipole model magnet," *IEEE Trans. Magn.*, vol. 32, no. 4, pp. 2097–2100, Jul. 1996.

[22] D. Leroy, G. Spigo, A. P. Verweij, H. Boschman, R. Dubbeldam, and J. G. Pelayo, "Design and manufacture of a large-bore 10 T superconducting dipole for the CERN cable test facility," *IEEE Trans. Appl. Supercond.*, vol. 10, no. 1, pp. 178–182, Mar. 2000.

[23] P. Vedrine et al., "The whole body 11.7 T MRI magnet for Iseult/INUMAC project," *IEEE Trans. Appl. Supercond.*, vol. 18, no. 2, pp. 868–873, Jun. 2008.

[24] L. Quettier et al., "Commissioning completion of the Iseult whole body 11.7 T MRI system," *IEEE Trans. Appl. Supercond.*, vol. 30, no. 4, Jun. 2020, Art. no. 4401705.

[25] S. Wenger, F. Zerobin, and A. Asner, "Towards a 1 m high field Nb/sub 3/Sn dipole magnet of the ELIN-CERN collaboration for the LHC-project-development and technological aspects," *IEEE Trans. Appl. Supercond.*, vol. 25, no. 2, pp. 1636–1639, Mar. 1989.

[26] A. Den Ouden, S. Wessel, E. Krooshoop and H. ten Kate, "Application of $Nb_3Sn$ superconductors in high-field accelerator magnets," *IEEE Trans. Appl. Supercond.*, vol. 7, no. 2, pp. 733–738, Jun. 1997.

[27] D. Dell'Orco, R. Scanlan, and C. E. Taylor, "Design of the $Nb_3Sn$ dipole D20," *IEEE Trans. Appl. Supercond.*, vol. 3, no. 1, pp. 82–86, Mar. 1993.

[28] A. D. McInturff et al., "Test results for a high field (13 T) Nb/sub 3/Sn dipole," in *Proc. Part. Accel. Conf.*, 1997, pp. 3212–3214.

[29] G. Sabbi et al., "Design of HD2: A 15 tesla $Nb_3Sn$ dipole with a 35 mm bore," *IEEE Trans. Appl. Supercond.*, vol. 15, no. 2, pp. 1128–1131, Jun. 2005.

[30] A. Milanese et al., "Design of the EuCARD high field model dipole magnet FRESCA2," *IEEE Trans. Appl. Supercond.*, vol. 22, no. 3, Jun. 2012, Art. no. 4002604.

[31] G. Willering et al., "Tests of the FRESCA2 100 mm bore $Nb_3Sn$ block-coil magnet to a record field of 14.6 T," *IEEE Trans. Appl. Supercond.*, vol. 29, no. 5, Aug. 2019, Art. no. 4004906.

[32] O. Brüning et al., "LHC luminosity and energy upgrade: A feasibility study," European Organization For Nuclear Research, Geneva, Switzerland, LHC Project Rep. 626, Dec. 2002.

[33] O. Bruning and L. Rossi, *The High-Luminosity Large Hadron Collider*. Singapore: World Scientific, Oct. 2015.

[34] E. Todesco et al., "A first baseline for the magnets in the high luminosity LHC insertion regions," *IEEE Trans. Appl. Supercond.*, vol. 24, no. 3, Jun. 2014, Art. no. 4003305.

[35] P. Ferracin et al., "Development of MQXF: The $Nb_3Sn$ low-$\beta$ quadrupole for the HiLumi LHC," *IEEE Trans. Appl. Supercond.*, vol. 26, no. 4, Jun. 2016, Art. no. 4000207.

[36] E. Todesco et al., "The high luminosity LHC interaction region magnets towards series production," *Supercond. Sci. Technol.*, vol. 34, no. 5, Mar. 2021, Art. no. 053001.

[37] S. A. Gourlay et al., "Magnet R&D for the US LHC accelerator research program (LARP)," *IEEE Trans. Appl. Supercond.*, vol. 16, no. 2, pp. 324–327, Jun. 2006.

[38] S. Caspi and P. Ferracin, "limits of $Nb_3Sn$ accelerator magnets," in *Proc. Part. Accel. Conf.*, 2005, pp. 107–111.

[39] R. C. Bossert et al., "Development of TQC01, a 90 mm $Nb_3Sn$ Model quadrupole for LHC upgrade based on SS collar," *IEEE Trans. Appl. Supercond.*, vol. 16, no. 2, pp. 370–373, Jun. 2006.

[40] S. Caspi et al., "Design and analysis of TQS01, a 90 mm $Nb_3Sn$ model quadrupole for LHC luminosity upgrade based on a key and bladder assembly," *IEEE Trans. Appl. Supercond.*, vol. 16, no. 1, pp. 358–361, Jun. 2006.

[41] S. Caspi et al., "The use of pressurized bladders for stress control of superconducting magnets," *IEEE Trans. Appl. Supercond.*, vol. 11, no. 1, pp. 2272–2275, Mar. 2001.

[42] S. Caspi et al., "Design of a 120 mm bore 15 T quadrupole for the LHC upgrade phase II," *IEEE Trans. Appl. Supercond.*, vol. 20, no. 3, pp. 144–147, Jun. 2010.

[43] G. Ambrosio et al., "Design of $Nb_3Sn$ Coils for LARP long magnets," *IEEE Trans. Appl. Supercond.*, vol. 17, no. 2, pp. 1035–1038, Jun. 2007.

[44] G. Chlachidze et al., "Performance of the first short model 150-mm-aperture Nb3Sn quadrupole MQXFS for the high-luminosity LHC upgrade," *IEEE Trans. Appl. Supercond.*, vol. 27, no. 4, Jun. 2017, Art. no. 4000205.

[45] G. Ambrosio et al., "Challenges and lessons learned from fabrication, testing, and analysis of eight MQXFA low beta quadrupole magnets for HL-LHC," *IEEE Trans. Appl. Supercond.*, vol. 33, no. 5, Aug. 2023, Art. no. 4003508.

[46] S. I. Bermudez et al., "Status of the MQXFB $Nb_3Sn$ quadrupoles for the HL-LHC," *IEEE Trans. Appl. Supercond.*, vol. 33, no. 5, Aug. 2023, Art. no. 4001209.

[47] S. Stoynev et al., "Summary of test results of MQXFS1 - the first short model 150 mm aperture $Nb_3Sn$ quadrupole for the high-luminosity LHC upgrade," *IEEE Trans. Appl. Supercond.*, vol. 28, no. 3, Apr. 2018, Art. no. 4001705.

[48] S. I. Bermudez et al., "Performance of a MQXF $Nb_3Sn$ quadrupole magnet under different stress level," *IEEE Trans. Appl. Supercond.*, vol. 32, no. 6, Sep. 2022, Art. no. 4007106.

[49] F. J. Mangiarotti et al., "Performance of HL-LHC $Nb_3Sn$ quadrupole magnet in the 100–200 MPa range of azimuthal stress," *IEEE Trans. Appl. Supercond.*, vol. 35, no. 5, Aug. 2025, Art. no. 4000307.

[50] A. Moros et al., "A metallurgical inspection method to assess the damage in performance limiting $Nb_3Sn$ accelerator magnets," *IEEE Trans. Appl. Supercond.*, vol. 33, no. 5, Aug. 2023, Art. no. 4000208.

[51] I. Santillana et al., "Advanced examination of $Nb_3Sn$ coils and conductors for the LHC luminosity upgrade: A methodology based on computed tomography and materialographic analyses," *Supercond. Sci. Technol.*, vol. 37, no. 8, Jul. 2024, Art. no. 085007.

[52] E. Ravaioli et al., "First experience with the new coupling loss induced quench system," *Cryogenics*, vol. 60, pp. 33–43, 2014.

[53] E. Ravaioli et al., "Quench protection performance measurements in the first MQXF magnet models," *IEEE Trans. Appl. Supercond.*, vol. 28, no. 3, Apr. 2018, Art. no. 4701606.

[54] M. Bajko et al., "HL-LHC IT STRING: Status and perspectives," *IEEE Trans. Appl. Supercond.*, vol. 34, no. 5, Aug. 2024, Art. no. 9001306.

[55] M. Benedikt, "FCC-hh: The hadron collider," *Eur. Phys. J.*, vol. 228, no. 4, pp. 834–845, Jul. 2019.

[56] The CEPC-SPPC study group, "CEPC-SppC preliminary conceptual design report," HEP-CEPC-DR-2015-01 IHEP-AC-2015-01, Mar. 2015.

[57] D. Tommasini et al., "The 16 T dipole development program for FCC," *IEEE Trans. Appl. Supercond.*, vol. 27, no. 4, Jun. 2017, Art. no. 4000405.

[58] A. Ballarino et al., "The CERN FCC conductor development program: A world wide effort for the future generation of high field magnets," *IEEE Trans. Appl. Supercond.*, vol. 29, no. 5, Aug. 2019, Art. no. 6001709.

[59] M. Karppinen et al., "Design of 11 T twin-aperture $Nb_3Sn$ dipole demonstrator magnet for LHC upgrades," *IEEE Trans. Appl. Supercond.*, vol. 22, no. 3, Jun. 2012, Art. no. 4901504.

[60] E. Todesco et al., "Progress on HL-LHC $Nb_3Sn$ magnets," *IEEE Trans. Appl. Supercond.*, vol. 28, no. 4, Jun. 2018, Art. no. 4008809.

[61] A. V. Zlobin et al., "Development and test of a single-aperture 11 T $Nb_3Sn$ demonstrator dipole for LHC upgrades," *IEEE Trans. Appl. Supercond.*, vol. 23, no. 3, Jun. 2013, Art. no. 4000904.

[62] A. V. Zlobin et al., "Development and first test of the 15 T $Nb_3Sn$ dipole demonstrator MDPCT1," *IEEE Trans. Appl. Supercond.*, vol. 30, no. 4, Jun. 2020, Art. no. 4000805.

[63] S. Stoynev et al., "MDPCT1 Quench data and performance analysis," *IEEE Trans. Appl. Supercond.*, vol. 32, no. 6, Sep. 2022, Art. no. 4000705.

[64] R. Valente et al., "Electromagnetic and mechanical study for the $Nb_3Sn$ cos-theta dipole model for the FCC," *IEEE Trans. Appl. Supercond.*, vol. 30, no. 4, Jun. 2020, Art. no. 4001905.

[65] M. Mesci et al., "Mechanical design of the 12 T superconducting dipole, an accelerator-fit $Nb_3Sn$ double aperture magnet," in *Proc. Int. Part. Accel. Conf.*, 2024, pp. 2843–2846.

[66] S. I. Bermudez, R. Ortwein, J. C. Perez, and E. Rochepault, "Design of ERMC and RMM, the base of the $Nb_3Sn$ 16 T magnet development at CERN," *IEEE Trans. Appl. Supercond.*, vol. 27, no. 4, Jun. 2017, Art. no. 4002004.

[67] E. Gautheron et al., "Assembly and test results of the RMM1a,b magnet, a CERN technology demonstrator towards $Nb_3Sn$ ultimate performance," *IEEE Trans. Appl. Supercond.*, vol. 33, no. 5, Aug. 2023, Art. no. 4004108.

[68] J. C. Perez et al., "BOND: A 14 T dipole based on block coils," *IEEE Trans. Appl. Supercond.*, vol. 35, no. 5, Aug. 2025, Art. no. 4002506.

[69] H. Felice et al., "F2D2: A block-coil short-model dipole toward FCC," *IEEE Trans. Appl. Supercond.*, vol. 29, no. 5, Aug. 2019, Art. no. 4001807.

[70] R. Gupta, "A common coil design for high field 2-in-1 accelerator magnets," in *Proc. Int. Part. Accel. Conf.*, 1997, pp. 3344–3346.

[71] C. Wang et al., "Development of superconducting model dipole magnets beyond 12 T with a combined common-coil configuration," *Supercond. Sci. Technol.*, vol. 34, no. 6, Jun. 2023, Art. no. 065006.

[72] C. Wang et al., "Design and fabrication of a 13-T twin-aperture superconducting dipole magnet with graded common-coil configuration," *IEEE Trans. Appl. Supercond.*, vol. 34, no. 5, Aug. 2024, Art. no. 4000805.

[73] J. A. García-Matos, C. M. Jardim, F. Toral, S. I. Bermudez, and J. C. Perez, "Design of a common coil magnet using existing racetrack model coils (RMC)," *IEEE Trans. Appl. Supercond.*, vol. 34, no. 5, Aug. 2024, Art. no. 4300105.

[74] E. Todesco et al., "Analytical estimates of stress in superconducting dipole magnets for particle accelerators," submitted to Supercond. Sci. Technol.

[75] T. Elliot et al., "16 tesla Nb/sub 3/Sn dipole development at Texas A&M University," *IEEE Trans. Appl. Supercond.*, vol. 7, no. 2, pp. 555–557, Jun. 1997.

[76] S. Caspi et al., "Canted–Cosine–Theta magnet (CCT)—A concept for high field accelerator magnets," *IEEE Trans. Appl. Supercond.*, vol. 24, no. 3, Jun. 2014, Art. no. 4001804.

[77] P. Ferracin et al., "Conceptual design of 20 T hybrid accelerator dipole magnets," *IEEE Trans. Appl. Supercond.*, vol. 33, no. 3, Aug. 2023, Art. no. 4002007.

[78] I. Novitski et al., "Development and test of a large-aperture $Nb_3Sn$ cos-theta dipole coil with stress management," *IEEE Trans. Appl. Supercond.*, vol. 34, no. 5, Aug. 2023, Art. no. 4001305.

[79] D. I. Meyer and R. Flashck, "A new configuration for a dipole magnet for use in high energy physics applications," *Nucl. Instrum. Methods*, vol. 80, no. 2, pp. 339–341, Apr. 1970.

[80] D. Arbalez et al., "Status of the $Nb_3Sn$ canted-cosine-theta dipole magnet Program at Lawrence Berkeley national laboratory," *IEEE Trans. Appl. Supercond.*, vol. 32, no. 6, Sep. 2022, Art. no. 4003207.

[81] B. Auchmann et al., "Test results from CD1 short CCT Nb3Sn dipole demonstrator and considerations about CCT technology for the FCC-Hh main dipole," *IEEE Trans. Appl. Supercond.*, vol. 34, no. 5, Aug. 2024, Art. no. 4000906.

[82] P. Lee, "Page of plots available in the NHFML web site," Jan. 2025. [Online]. Available: https://nationalmaglab.org/magnet-development/applied-superconductivity-center/plots/

[83] D. C. Larbalestier et al., "High-$T_c$ superconducting materials for electric power applications," *Nature*, vol. 414, pp. 368–377, 2002.

[84] S. R. Foltyn et al., "Materials science challenges for high-temperature superconducting wire," *Nature Mater.*, vol. 6, pp. 631–642, 2007.

[85] G. Biswal, "A recent review on iron-based superconductor," *Mater. Today: Proc.*, vol. 35, pp. 207–215, 2021.

[86] G. R. Stewart, "Superconductivity in iron compounds," *Rev. Mod. Phys.*, vol. 83, no. 4, pp. 1589–1652, 2011.

[87] L. Rossi et al., "The EuCARD-2 future magnets European collaboration for accelerator-quality HTS magnets," *IEEE Trans. Appl. Supercond.*, vol. 25, no. 3, Jun. 2015, Art. no. 4001007.

[88] M. Durante et al., "Realization and first test results of the EuCARD 5.4-T REBCO dipole magnet," *IEEE Trans. Appl. Supercond.*, vol. 28, no. 3, Apr. 2018, Art. no. 4203805.

[89] M. Durante, P. Fazilleau, T. Lecrevisse, C. Lorin, M. Segreti, and O. Tellier, "Overview of HTS accelerator magnet developments at CEA Saclay," *IEEE Trans. Appl. Supercond.*, vol. 34, no. 5, Aug. 2024, Art. no. 4002905.

[90] G. A. Kirby et al., "First cold powering test of REBCO Roebel wound coil for the EuCARD2 Future Magnet Development Project," *IEEE Trans. Appl. Supercond.*, vol. 27, no. 4, Jun. 2017, Art. no. 4003307.

[91] L. Rossi and C. Senatore, "HTS Accelerator magnet and conductor development in European," *Instruments*, vol. 5, Jun. 2021, Art. no. 8.

[92] T. Shen et al., "Design, fabrication, and characterization of a high-field high-temperature superconducting Bi-2212 accelerator dipole magnet," *Phys. Rev. Accelerators Beams*, vol. 25, 2022, Art. no. 122401.

[93] X. Wang et al., "Development and performance of a 2.9 tesla dipole magnet using high-temperature superconducting CORC wires," *Supercond. Sci. Technol.*, vol. 34, 2021, Art. no. 015012.